(12)

OSU

The Ohio State University

NCTR USING A POLARIZATION-AGILE COHERENT RADAR SYSTEM

E.K. Walton
D.L. Moffatt
F.D. Garber
A. Kamis
C.Y. Lai

The Ohio State University

ElectroScience Laboratory

Department of Electrical Engineering
Columbus, Ohio 43212

Final Report 716559-2
Contract No. N00014-84-K-0705
January 1986

Office of Naval Research
800 N. Quincy St.
Arlington, VA 22217

NOTICES

When Government drawings, specifications, or other data are used for any purpose other than in connection with a definitely related Government procurement operation, the United States Government thereby incurs no responsibility nor any obligation whatsoever, and the fact that the Government may have formulated, furnished, or in any way supplied the said drawings, specifications, or other data, is not to be regarded by implication or otherwise as in any manner licensing the holder or any other person or corporation, or conveying any rights or permission to manufacture, use, or sell any patented invention that may in any way be related thereto.

50272-101

REPORT DOCUMENTATION PAGE	1. REPORT NO. 716559-2 AD-A163528	Recipient's Accession No

4. Title and Subtitle

NCTR USING A POLARIZATION-AGILE COHERENT RADAR SYSTEM

5. Report Date: January 1986

6.

7. Author(s): E.K. Walton, D.L. Moffatt, F.D. Garber, A. Kamis, C.Y. Lai

8. Performing Organization Rept. No. 716559-2

9. Performing Organization Name and Address

The ElectroScience Laboratory
The Ohio State University
1320 Kinnear Rd.
Columbus, Ohio 43212

10. Project/Task/Work Unit No.

11. Contract(C) or Grant(G) No
(C) N00014-84-K-0705
(G)

12. Sponsoring Organization Name and Address

Office of Naval Research
800 N. Quincy St.
Arlington, VA 22217

13. Type of Report & Period Covered: Final

14.

15. Supplementary Notes

16. Abstract (Limit: 200 words)

The goal of this research project is to study the use of the polarization properties of the signal scattered from a radar target for the purpose of radar target classification or identification. The research involves the application of a large data base derived from scale model measurements using the Ohio State University Compact Radar Measurement Range. The data base has been combined with a set of polarization state transformation algorithms to permit the testing of NCTR algorithms as a function of polarization. Also studied is the application of complex natural resonance techniques to the scattering data for various polarization states.

It is shown that co-polarized fully coherent radar systems with multifrequency capability can perform very effectly as NCTR systems. Signal-to-noise-ratios from 0 to +10 dB in the final estimate of the RCS and relative signal phase for the various targets is shown to be sufficient for misclassification percentages less than 5 percent. It is also shown that natural resonance data can be meaningfully utilized when applied to resonance region RCS data.

17. Document Analysis a. Descriptors

resonance region
NCTR
polarization
RCS measurements
radar
target classification
target identification
natural resonances

b. Identifiers/Open-Ended Terms

c. COSATI Field/Group

18. Availability Statement	19. Security Class (This Report)	21. No. of Pages
APPROVED FOR PUBLIC RELEASE; DISTRIBUTION IS UNLIMITED.	Unclassified	60
	20. Security Class (This Page) Unclassified	22. Price

(See ANSI-Z39.18) See Instructions on Reverse

OPTIONAL FORM 272 (4-77)
(Formerly NTIS-35)
Department of Commerce

TABLE OF CONTENTS

LIST OF TABLES

LIST OF FIGURES

CHAPTER 1

INTRODUCTION

This report describes the results of the first year of a research project performed by the Ohio State University ElectroScience Laboratory (OSU/ESL) for the Naval Weapons Center (NWC). The goal of this project is to explore the use of the polarization properties of the signal scattered from a radar target for the purpose of radar target identification. Various radar target identification algorithms were applied to the case of a full polarization coherent radar system, and were tested using a specific data base and noise model.

The data base used to test the performance of the radar target identification algorithms developed here is a unique set of measurements made on scale models of aircraft. Measurements were made using the OSU/ESL Compact Radar Measurement Range [1]. The range was operated in a broad-band (1-12 GHZ) mode and the full polarization matrix was measured. Calibrated values (amplitude and phase) of the RCS for the three polarization states were thus available. The polarization states are listed below.

INTRINSIC POLARIZATION STATES OF THE RCS MEASUREMENT SYSTEM

1. VV...transmit vertical polarization; receive vertical polarization
2. HH...transmit horizontal polarization; receive horizontal polarization
3. HV...transmit horizontal polarization; receive vertical polarization

The models used were plastic scale models of modern commercial aircraft which were silver coated using a dipping/plating process. The scale factor was approximately 200, which put the full scale frequency range in the 5 MHZ to 60 MHZ frequency band. This frequency/scale-factor relationship results in RCS values for the resonance region of the various aircraft. Aspect angles from 0 degrees (nose-on) to 180 degrees (tail-on) were used.

One of the first tasks was to develop the polarization state transformations and incorporate them into a computer data base manipulation program so that the polarization state could be derived from the original measurements and the resultant entered into radar target identification algorithms. This program, called RSSE, is described in ESL technical report 716559-1; which was prepared under this program to document the algorithms developed during this research [2]. During this phase of the research, a computer program which would display the polarization state of the signal scattered from the radar target on the well-known Poincaré sphere was developed. The Poincaré

projections for the various aircraft at various aspect angles and for various illumination polarization states proved to be very useful for gaining insight into the utilization of such a mapping for the development of other radar identification algorithms. Examples are given in Chapter 3.

The application of resonance-region radar target identification algorithms to the polarization-derived features is also demonstrated in Chapter 3. Tests of the performance of the various features in the radar target identification environment are shown and the results statistically compared. These comparisons of the various algorithms which utilize the various polarization dependent feature sets are used to summarize the results of this phase of the research in this area.

The other area which was studied is the application of complex natural resonance techniques to polarization states and frequency bands which were not available in the previous work. This research involves the extraction of the complex poles of the RCS signatures of the radar targets described in Chapter 2 of this report. The extracted poles are then used in specific radar target identification algorithms [3]. Statistics of the performance of these algorithms are given in Chapter 3.

CHAPTER 2

DATA BASE AND HANDLING

2.1 DATA-BASE DESCRIPTION

A critical prerequisite for performing the target identification research discussed below is the generation and maintanence of a well-organized, easily accessible data base containing the precise wide-band full-polarization scattering matrix measurements of a number of aircraft targets of interest. Due in large part to support from the Office of Naval Research (under contract N00014-82-K-0037), such a data base has been generated at the ElectroScience Laboratory using the compact radar range at ESL to measure the far-field radar backscatter returns from scale-models of five commercial aircraft including: the Concorde, Douglas DC-10, and the Boeing 707, 727, and 747.

The cross section measurements made on these scale-model aircraft were typically performed in the 1-12 GHz frequency band which, for a scale factor of 200:1 (say) corresponds to full-scale measurements from 5-60 MHz. These measurements were performed for each of the aircraft listed above for a number of azimuth angles of interest, using both linear co-pole configurations (HH and VV) as well as the linear cross-pole (HV) configurations of the compact range. Listings of the data-base entries for each aircraft, including the data-base file locations, the scale factor of the model employed, and the range of

available measurements (in GHz) for each polarization and azimuth (aspect) angle appear in Tables 1-5 [2]. In these tables, the entry "6-12" (for example) indicates that only measurements in the 6-12 GHz range are avialable for this aircraft at the particular polarization and azimuth angle. The entry "null" implies that no data are available for this target at this azimuth and polarization.

2.2 DATA-BASE HANDLING

Three software packages for data-base manipulation and processing were developed under support or partial support from this program; each performing a set of tasks of interest. The first package performs tasks related to data-base management, including generation, mapping, and any necessary modifications. The second performs polarization mappings and Fourier analyses of original and transformed parameters. The third software package developed under the sponsorship of this program allows the investigation of the performance of various radar target identification systems based on different types and ranges of features.

A complete description of the use and capabilities of these computer subroutines appears in the earlier report from this project [2]. Much of the discussion and data presented below are based on results obtained using one or more of these software packages.

TABLE 2.1

DATA BASE ENTRIES FOR BOEING 707

MAPPING DATABASE :

707

TITLE : 707 AIRPLANE

CALIBRATED FILES FROM DISK PACK ONR7 DIRECTORY 707
DBM HEADER FILE DLA0:[ONR7.707]707CAL.DBM
SCALE FACTOR = 150.0 ELEVATION ANGLE = 0 DEGREES

FREQUENCY FORMATTED DATA BASE (GHz)

ASPECT (Deg)	POLARIZATION		
	HH	HV	VV
0	1-12	1-12	1-12
10	1-12	NULL	1-12
15	1-12	1-12	1-12
20	1-12	1-12	1-12
25	6-12	NULL	6-12
30	1-12	1-12	1-6.3
35	6-12	NULL	6-12
40	1-12	1-12	1-12
45	1-12	1-12	1-12
50	1-12	1-12	1-12
55	6-12	NULL	6-12
60	1-12	1-12	1-12
65	6-12	NULL	6-12
70	1-12	1-12	1-12
75	1-12	1-12	1-12
80	1-12	1-12	1-12
85	6-12	NULL	6-12
90	1-12	1-12	1-12
95	6-12	NULL	6-12
100	1-12	1-12	1-12
105	1-12	1-12	1-12
110	1-12	1-12	1-12
115	6-12	NULL	6-12
120	1-12	1-12	1-12
125	6-12	NULL	6-12
130	1-12	1-12	1-12
135	1-12	1-12	1-12
140	1-12	1-12	1-12
145	6-12	NULL	6-12
150	1-12	1-12	1-12
155	6-12	NULL	6-12
160	1-12	1-12	1-12
165	1-12	1-12	1-12
170	1-12	1-12	1-12
175	6-12	NULL	6-12
180	1-12	1-12	1-12
270	6-12	NULL	1-12

TABLE 2.2

DATA BASE ENTRIES FOR BOEING 727

MAPPING DATABASE :

727

TITLE : 727 AIRPLANE 9 INCH 727

CALIBRATED FILES FROM DISK PACK ONR1 DIRECTORY 727
DBM HEADER FILE DLA0:[ONR1.727]727CAL.DBM
SCALE FACTOR = 200.0 ELEVATION ANGLE = 0 DEGREES

FREQUENCY FORMATTED DATA BASE (GHz)

ASPECT (Deg)	POLARIZATION		
	* HH *	* HV *	* VV *
0	1-12	1-12	1-12
10	1-12	1-12	1-12
15	1-12	1-12	1-12
20	1-12	1-12	1-12
30	1-12	1-12	1-12
40	1-12	1-12	1-12
45	1-12	1-12	1-12
50	1-12	1-12	1-12
60	1-12	1-12	1-12
70	1-12	1-12	1-12
75	1-12	1-12	1-12
80	1-12	1-12	1-12
90	1-12	1-12	1-12
100	1-12	1-12	1-12
105	1-12	1-12	1-12
110	1-12	1-12	1-12
120	1-12	1-12	1-12
130	1-12	1-12	1-12
135	1-12	1-12	1-12
140	1-12	1-12	1-12
150	1-12	1-12	1-12
160	1-12	1-12	1-12
165	1-12	1-12	1-12
170	1-12	1-12	1-12
180	1-12	1-12	1-12
270	1-12	1-12	1-12

TABLE 2.3

DATA BASE ENTRIES FOR BOEING 747

MAPPING DATABASE :

747

TITLE : 747 AIRPLANE LARGE 747

CALIBRATED FILES FROM DISK PACK ONR4 DIRECTORY 747
DBM HEADER FILE DLA0:[ONR4.747]747CAL.DBM
SCALE FACTOR = 200.0 ELEVATION ANGLE = 0 DEGREES

FREQUENCY FORMATTED DATA BASE (GHz)

ASPECT (Deg)	POLARIZATION		
	* HH *	* HV *	* VV *
0	1.5-12	1-12	1-12
10	1.5-12	1-12	NULL
15	6-12	1-12	1-12
20	1.5-12	1-12	NULL
25	6-12	NULL	NULL
30	1.5-12	1-12	1-12
35	6-12	NULL	NULL
40	1.5-12	1-12	NULL
45	1.5-12	1-12	1-12
50	1.5-12	1-12	NULL
55	6-12	NULL	NULL
60	1.5-12	1-12	1-12
65	6-12	NULL	NULL
70	1.5-12	1-12	NULL
75	6-12	1-12	1-12
80	1.5-12	1-12	NULL
90	1.5-12	1-12	1-12
95	6-12	NULL	NULL
100	1.5-12	1-12	NULL
105	6-12	1-12	1-12
110	1.5-12	1-12	NULL
115	6-12	NULL	NULL
120	1.5-12	1-12	1-12
125	6-12	NULL	NULL
130	1.5-12	1-12	NULL
135	6-12	1-12	1-12
140	1.5-12	1-12	NULL
145	6-12	NULL	NULL
150	1.5-12	1-12	1-12
155	6-12	NULL	NULL
160	1.5-12	1-12	NULL
165	6-12	1-12	1-12
170	1.5-12	1-12	NULL
180	1.5-12	1-12	1-12

TARLE 2.4

DATA BASE ENTRIES FOR THE CONCORDE

MAPPING DATABASE :

CON

TITLE : CONCORD AIRPLANE LARGE CONCORD

CALIBRATED FILES FROM DISK PACK ONR1 DIRECTORY CON
DBM HEADER FILE DLW0:[ONR1.CON]CONCAL.DBM
SCALE FACTOR = 130.0 ELEVATION ANGLE = 0 DEGREES

FREQUENCY FORMATTED DATA BASE (GHz)

ASPECT (Deg)	POLARIZATION		
	HH	HV	VV
0	1-12	1-12	1-12
10	1-12	1-12	1-12
15	1-12	NULL	1-12
20	1-12	1-12	1-12
25	6-12	NULL	6-12
30	1-12	1-12	1-12
35	6-12	NULL	6-12
40	1-12	1-12	1-12
45	1-12	1-12	1-12
50	1-12	1-12	1-12
55	6-12	NULL	6-12
60	1-12	1-12	1-12
65	6-12	NULL	6-12
70	1-12	1-12	1-12
75	1-12	1-12	1-12
80	1-12	1-12	1-12
85	6-12	NULL	6-12
90	1-12	1-12	1-12
95	6-12	NULL	6-12
100	1-12	1-12	1-12
105	1-12	1-12	1-12
110	1-12	1-12	1-12
115	6-12	NULL	6-12
120	1-12	1-12	1-12
125	6-12	NULL	6-12
130	1-12	1-12	1-12
135	1-12	1-12	1-12
140	1-12	1-12	1-12
145	6-12	NULL	6-12
150	1-12	1-12	1-12
155	6-12	NULL	6-12
160	1-12	1-12	1-12
165	1-12	1-12	1-12
170	1-12	1-12	1-12
175	6-12	NULL	6-12
180	1-12	1-12	1-12

TABLE 2.5

DATA BASE ENTRIES FOR DC10

MAPPING DATABASE :

DC10

TITLE : DC10 AIRPLANE ELEVEN INCH DC10

CALIBRATED FILES FROM DISK PACK ONR7 DIRECTORY DC10
DBM HEADER FILE DLA0:[ONR7.DC10]DC10CAL.DBM
SCALE FACTOR = 200.0 ELEVATION ANGLE = 0 DEGREES

FREQUENCY FORMATTED DATA BASE (GHz)

ASPECT (Deg)	POLARIZATION		
	HH	HV	VV
10	1-12	1-12	1-12
15	1-12	1-12	1-12
20	1-12	1-12	1-12
30	1-12	1-12	1-12
40	1-12	1-12	1-12
45	1-12	1-12	1-12
50	1-12	1-12	1-12
60	1-12	1-12	1-12
70	1-12	1-12	1-12
75	1-12	1-12	1-12
80	1-12	1-12	1-12
90	1-12	1-12	1-12
100	1-12	1-12	1-12
105	1-12	1-12	1-12
110	1-12	1-12	1-12
120	1-12	NULL	1-12
130	1-12	NULL	1-12
135	1-12	NULL	1-12
140	1-12	1-12	1-12
150	1-12	1-12	1-12
160	1-12	1-12	1-12
165	1-12	1-12	1-12
170	1-12	1-12	1-12
180	1-12	1-12	1-12
270	1-12	1-12	1-12

CHAPTER 3

FULL SCATTERING MATRIX TARGET ID RESEARCH

3.1 INTRODUCTION

Several investigators have suggested that data containing the broad-band measurements of the full polarization scattering matrix for a set of targets would contain a great deal of information useful for target identification algorithms [4]; however, until recently, precise measurements for all but canonical targets were not available and target identification techniques based on polarization-intensive information could not be evaluated for practical radar targets.

The primary focus of the research described in this report, and the motivation for the generation of the data base and handling software discussed above, was the investigation of the performance of radar target identification algorithms applied to the full polarization scattering matrix data for a set of five common aircraft. As a part of this study, the effects of additive white Gaussian noise on the performance of systems employing various polarizations and combinations of polarizations was investigated. Of particular interest were the initial comparisons of the performance of a nearest-neighbor algorithm using linear (HH, VV, and HV), circular (RR, LL, and RL), and axial-ratio polarization coefficients as features.

A secondary goal of this study was the assessment of the value of precise phase information in this particular additive noise environment. This was accomplished by performing simulation studies using both "coherent" (complex) and "non-coherent" (magnitude) distance metrics as part of the nearest-neighbor algorithm. In each case, the performance parameter of interest was the average percentage of misclassification as a function of the average power level of the noise.

In the following sections of this chapter, several of the key issues in polarization scattering matrix based target identification are discussed in more detail and the results obtained as part of this effort are presented and compared.

3.2 POLARIZATION STATE TRANSFORMATIONS

The data base contains the absolute amplitude and phase of the RCS of five different aircraft over a broad band of frequencies. Measurements were made using vertical and horizontal polarization states (VV-HH-VH). It is thus possible to transform from the linear polarization states to circular (or any elliptical polarization state). Listed below are several reasons for considering this type of transformation of the data prior to applying a target identification scheme.

- They are linear transformations; so the characteristics of the additive noise process will remain unchanged.

- Aircraft and missiles in particular tend to be symmetric bodies. Considering the head-on or tail-on aspect angle, it can be seen that a change in the roll angle of the aircraft will change the vertical and horizontal scattering components considerably, but will not change the circular scattering components except in the phase.
- The symmetry of aircraft and missiles also tends to transform the scattering matrix $[T]_{2x2}$ to a unitary matrix if the components are circularly polarized. Observe that in the nose or tail aspect zone, the symmetry of the aircraft or missile tends to make T_{12} and T_{21} equal to zero (as is also the case for linear components), and that it has the additional property of making T_{11} equal to T_{22}.
- Even in the non-symmetric aspect zones, aircraft or missile maneouvers will have less influence on the parameters of the circular polarization RCS components because components of rotation about the line of sight axis will not enter into the response variation.

With these considerations in mind, a polarization state transformation algorithm was implemented and comparisons of the target identification algorithm performance were made.

3.2.1 Linear To Circular Polarization Transformation

In general, a radar system including the radar target can be considered a two-port network problem. The relationships can be expressed as

$$\left[\underline{S}_R\right]_{1x2} = \left[\underline{S}_T\right]_{1x2} \left[\underline{I}\right]_{2x2} \tag{3.1}$$

or

$$\left[\underline{S}_1^R \;,\; \underline{S}_2^R\right] = \left[S_1^T \;,\; S_2^T\right] \begin{bmatrix} \underline{I}_{11} & \underline{I}_{12} \\ \underline{I}_{21} & \underline{I}_{22} \end{bmatrix} \tag{3.2}$$

Where $\underline{S}_R$ is the received signal, $\underline{S}_T$ is the transmitted signal, and $\underline{I}_{ij}$ expresses the relationship between them. In our case, $\underline{I}_{ij}$ is normalized to give the relationship in units of meters (i.e., the square root of the RCS in units of square meters). Since reciprocity holds here, $\underline{I}_{12}$ equals $\underline{I}_{21}$.

In these equations, the subscripts 1 or 2 indicates orthogonal polarization states. The relationships can be expressed in terms of any two orthogonal polarization states. There exist transformations between the various orthogonal polarization states, and we will use the transformations from linear states to circular states here. They are given as:

$$\underline{I}_{RR} = \frac{1}{2}\left(\underline{I}_{VV} - \underline{I}_{HH}\right) + j\underline{I}_{VH} \tag{3.3}$$

$$\underline{T}_{LL} = \frac{1}{2}(\underline{T}_{VV} - \underline{T}_{HH}) - j\underline{T}_{VH} \tag{3.4}$$

$$\underline{T}_{LR} = \underline{T}_{RL} = \frac{1}{2}(\underline{T}_{VV} + \underline{T}_{HH}) \tag{3.5}$$

In this case, the subscripts are defined as;

* R = right hand circular
* L = left hand circular
* V = vertical
* H = horizontal

Where $\underline{T}_{ij}$ are given in units of area (RCS) and phase with respect to a reference point near the center of the target.

These transformations have been implemented on the ElectroScience Laboratory VAX-11/780 computer to be compatable with the aircraft data base. The transformed results are then used as input to the target identification algorithms. This means that the input to the target identification algorithms can be any of the feature sets described below. (The program is documented in detail in report 716559-1 [2].)

Features available to the target ID algorithm

1. Radar Cross Section (calibrated amplitude and phase)
   * transmit vertical or horizontal and receive vertical or horizontal (VV - HH - VH or HV)
   * transmit right or left hand circular and receive right or left hand circular (RR - LL - RL or LR)

2. transmit right or left hand circular and measure the axial ratio of the received polarization ellipse (RAX - LAX)

Note the utilization of the received signal polarization axial ratio. This is computed from the orthogonal components of the received signal. If the received signal were displayed as a signal voltage in the plane perpendicular to the direction of propagation, the signal would trace out the well-known polarization ellipse. The ratio of the major to minor axis of this ellipse is the axial ratio referred to here.

Note that the polarization nulls are not used as a target identification feature. These parameters of the radar scattering from a target have the advantage that they are radar-independent features of the target (they <u>are</u> dependent on the pitch, roll and yaw of the target). They may be studied at some future date, but in terms of their information content and usefulness for target identification, there is no indication at this time that they will contain more features relevant to target identification than the direct measurements discussed here.

Examples of the use of the above features in the identification of the aircraft targets in the data base will be shown in the next section.

3.2.2 Poincaré Transformations

It is possible to display the measurements made on the aircraft data base on the well-known Poincaré sphere. In this case, the

polarization state of the received signal for various transmitted signal polarizations is presented as a point plotted on the surface of a sphere. An example of the Poincaré sphere is shown in Figure 3.1. This figure shows the relationship between α, β, γ and ϕ, where these parameters are listed below.

Poincaré parameters

* α = arctangent of ellipse axial ratio
* β = orientation of ellipse major axis
* γ = arctangent of the ratio of the vertical and horizontal components of the signal current magnitudes
* ϕ = electrical phase angle between the vertical and horizontal signal components

An example where the scattering from the Boeing 747 model has been transformed to show the variation of the tilt angle, the axial ratio and the intensity of the scattered signal for the case of left-hand circular illumination is shown in Figure 3.2. Note that these parameters are shown as a function of frequency over the measurement band from 1 to 12 GHz. Note that in this case, the target is viewed nose-on. This means that the aircraft is a symmetric radar target, and if the target had been illuminated with a left-hand circular transmitted signal, the

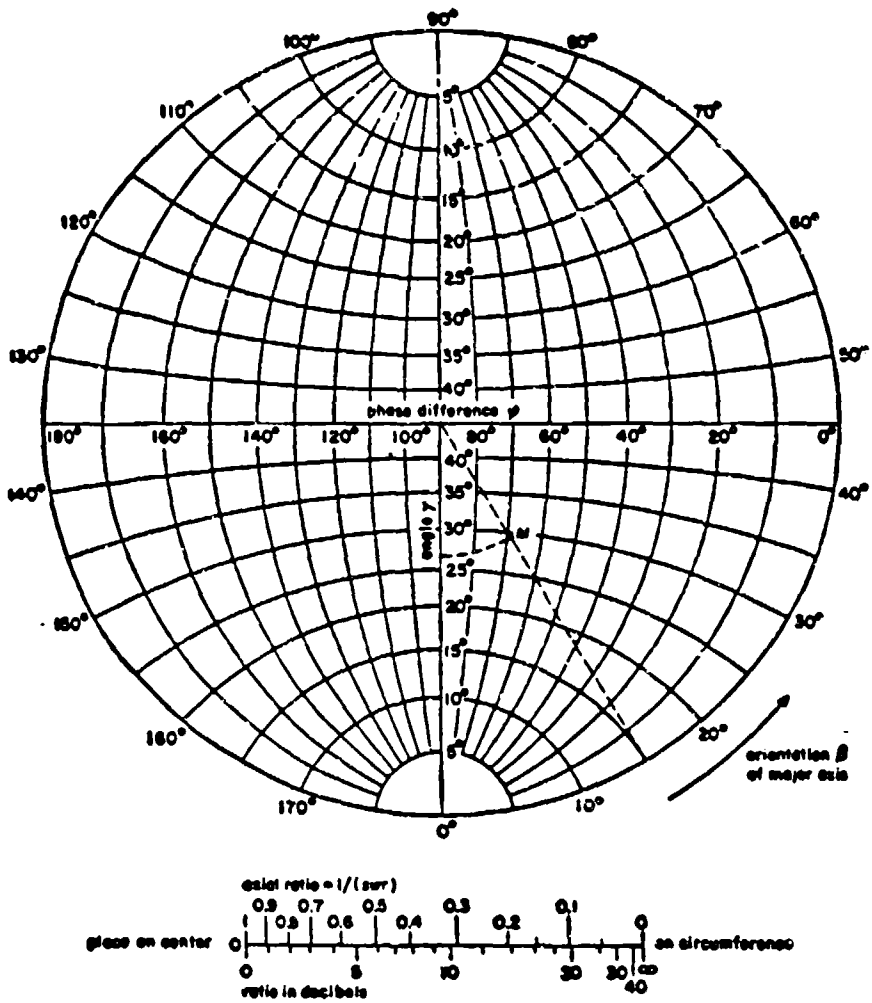

Figure 3.1. Polar projection of Poincaré sphere.

intensity would have been the same, but the axial ratio and the tilt angle would have been reversed. (These results were confirmed with the actual measured data.) The impact of this observation is that the number of independent variables is significantly reduced in this feature space. There is no reason to transmit the orthogonal circular polarization state for the nose-on (or tail-on) aspect angle because the resulting data will not contain any new information. If the roll angle of the target were to change, only the tilt angle parameter would change. Furthermore, this parameter would change in a predictable way (it would roll with the target). From the point of view of target identification, this means that the intensity and the axial ratio are quite stable as the aircraft rolls. From the point of view of radar signature analysis, this means that the roll angle of the target is contained in the tilt angle parameter. This may be a useful parameter for predicting the future position of the aircraft (or missile) since the aircraft is required to roll in order to initiate a turn.

A Poincaré plot of the parameteres shown in Figure 3.2 is shown in Figure 3.3. Note that the amplitude is indicated by the size of the symbol plotted at each point. The data proceeds from point to point as a function of frequency. Once again, the starting frequency was 1 GHz (marked with an "S" in the figure), the increment is 50 MHz, and the final frequency is 12 GHz (marked with an "F" on the figure). (The middle frequency (5.5 GHz) is marked with an "M" on the figure.)

Note that from the perspective of a human being, this is a messy plot. Certain topological patterns begin to emerge, however, as the

plot is studied. Note for example that the larger amplitude data falls into three clusters; one near linear horizontal, one near linear vertical and one near linear 45 degrees tilt angle. It can also be seen that the most common variation as a function of frequency is a variation in tilt angle. Automatic algorithms for the extractions of such parameters and their utilization in target identification schemes will be studied in the near future.

The key to the utilization of such features for target identificaton lies in the stability of these features for a given aircraft type and the variation of these features between different aircraft types. A set of examples where this property can be evaluated is shown in Figures 3.4 through 3.8. In these figures, the data from five aircraft are shown plotted as in Figure 3.3 but with a much smaller frequency extent. The frequencies were chosen so as to cover the same full-scale band (the 8 to 16 MHz band) for the various aircraft. Note that this frequency band covers a bandwidth of 8 MHz, which implys a range resolution of approximately 19 meters (61 feet), therefore, we are clearly not using a bandwidth large enough to resolve individual scattering centers. The target is behaving much like a lumped impedance transformer (ie: It generates an amplitude and phase response as a function of frequency, but such response does not resolve into discrete scattering centers.)

Note that the patterns seen in the data are simpler for human viewing but that a computer may be just as happy with the larger bandwidth data shown in Figure 3.3. Also note that the data tend to cluster the high amplitude components near the linear polarization state

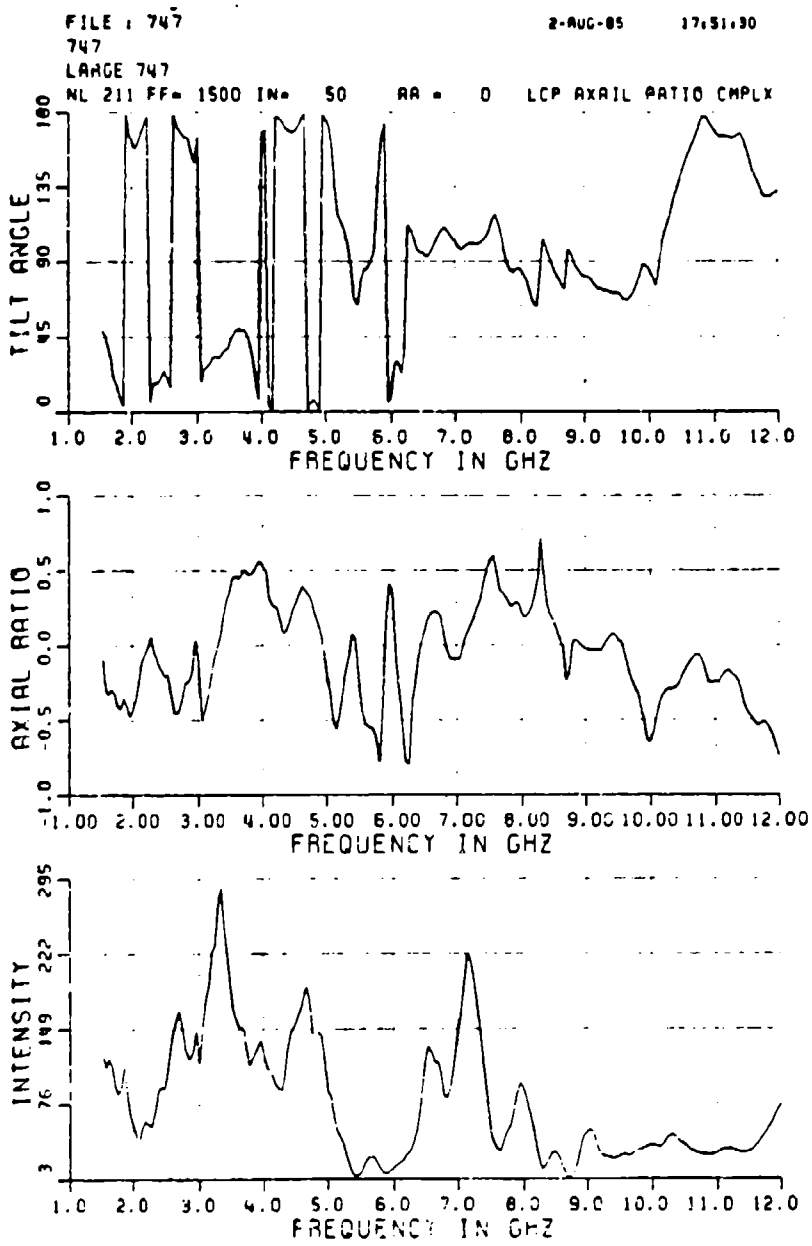

Figure 3.2. Polarization parameters for Boeing 747 as a function of frequency.

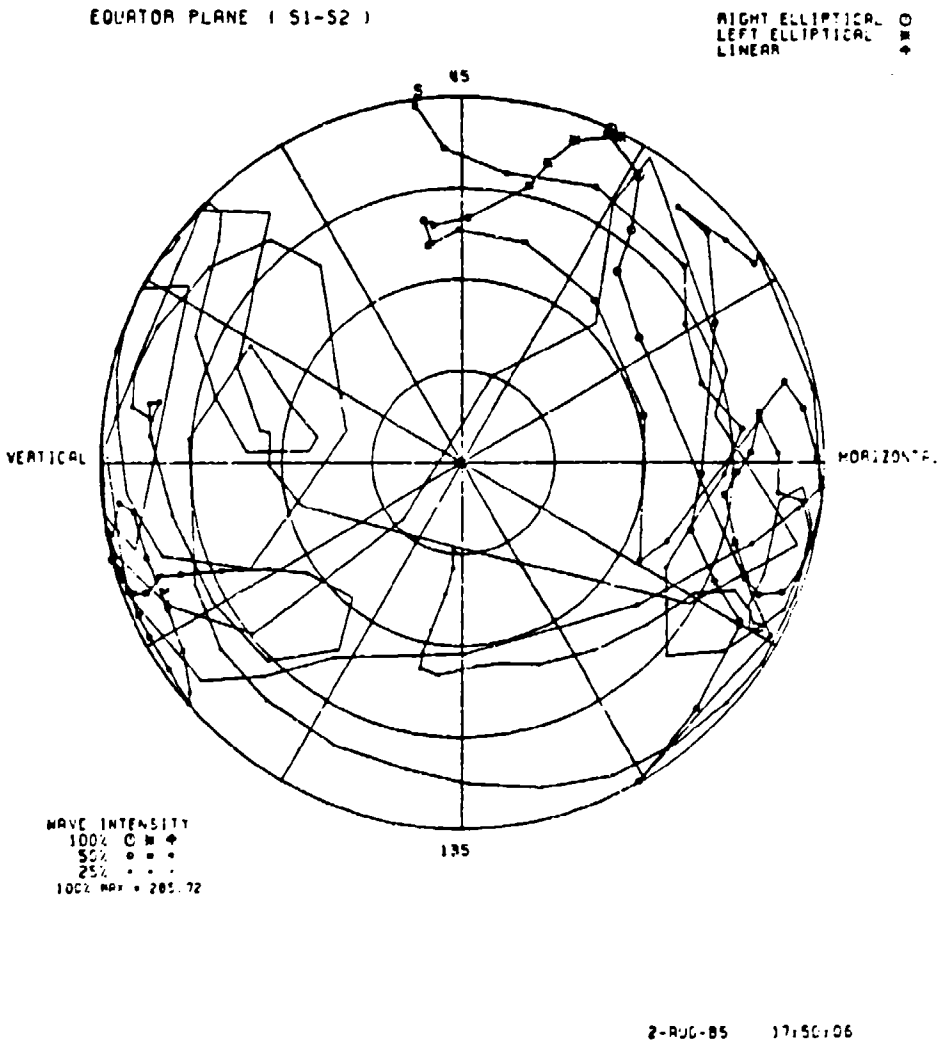

Figure 3.3. Polar projection of Poincaré sphere representation of scattering from Boeing 747.

for all of the models. An occasional "looping" pattern can also be seen in some of the data (the Concorde and the 727 for example). We have found that this is usually due to interference between multiple scattering centers on a target.

Of particular interest is the practicality of using these types of presentations to understand the behavior of the polarization state parameters as features for target identification. These patterns for the various aircraft can be seen to be uniquely different, and the task is to properly quantify these differences so that they can behave as features for a target identification system.

As an example of the separability of the various aircraft response curves in this parameter space, Figure 3.9 shows an estimate of the smoothed response of each of the aircraft plotted on a single Poincaré graph. Note that the various curves are uniquely different. A small set of data on an unknown target (from this group) would clearly be identifiable. An example where this has been done is shown in Figure 3.10. In this figure, the RCS of the various aircraft was plotted on the polar projection of the Poincaré sphere for the two orthogonal circular illumination cases. Only the starting frequency (S), the middle frequency (M) and the final frequency cases (F) are indicated. Note the wide separation of the various parameters. It can be expected that if the polarization states for an unknown aircraft were to be plotted on this curve, it would be possible to associate the unknown with a particular aircraft type. (We assume that the unknown aircraft is included in the "catalog".) Future research will focus on these concepts in an attempt to quantify these results, on the development of

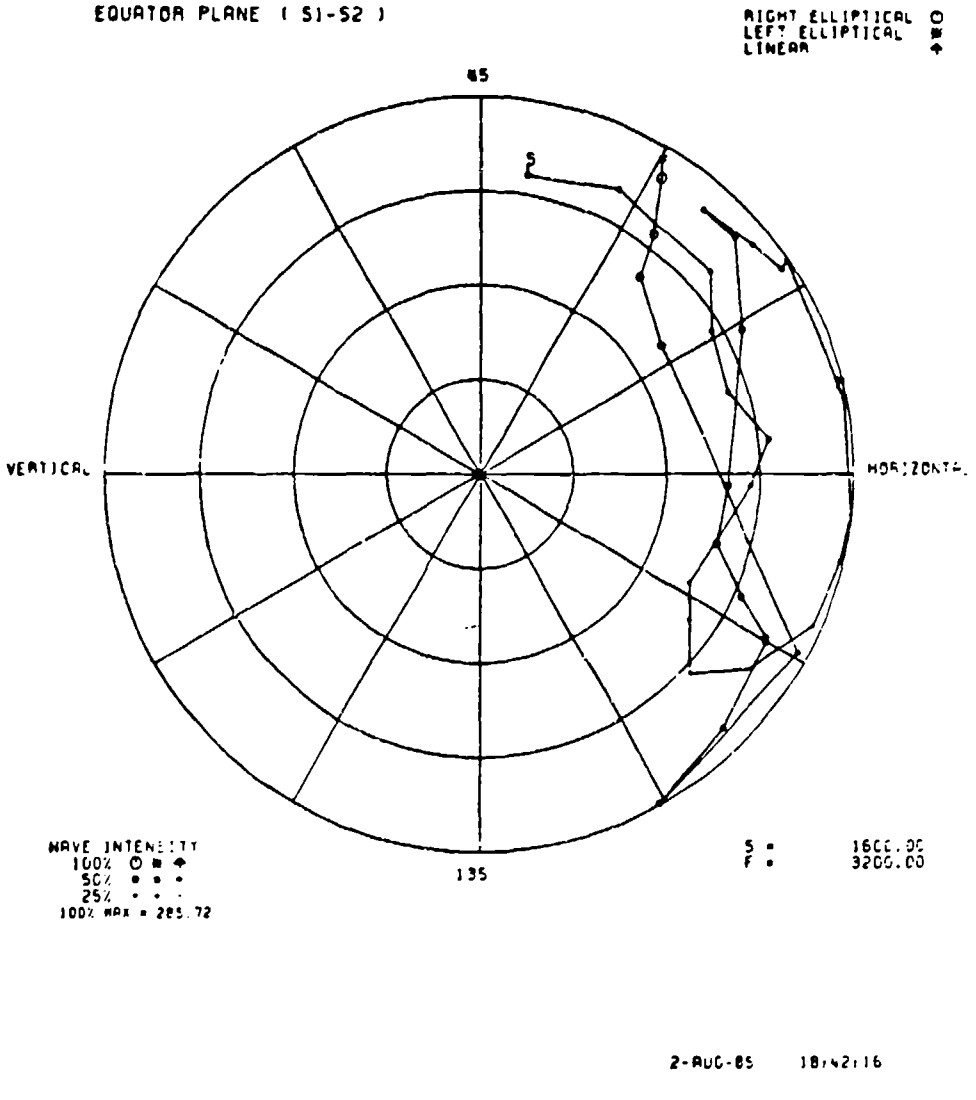

Figure 3.4. Polar projection of Poincaré sphere representation for Boeing 747 (band limited).

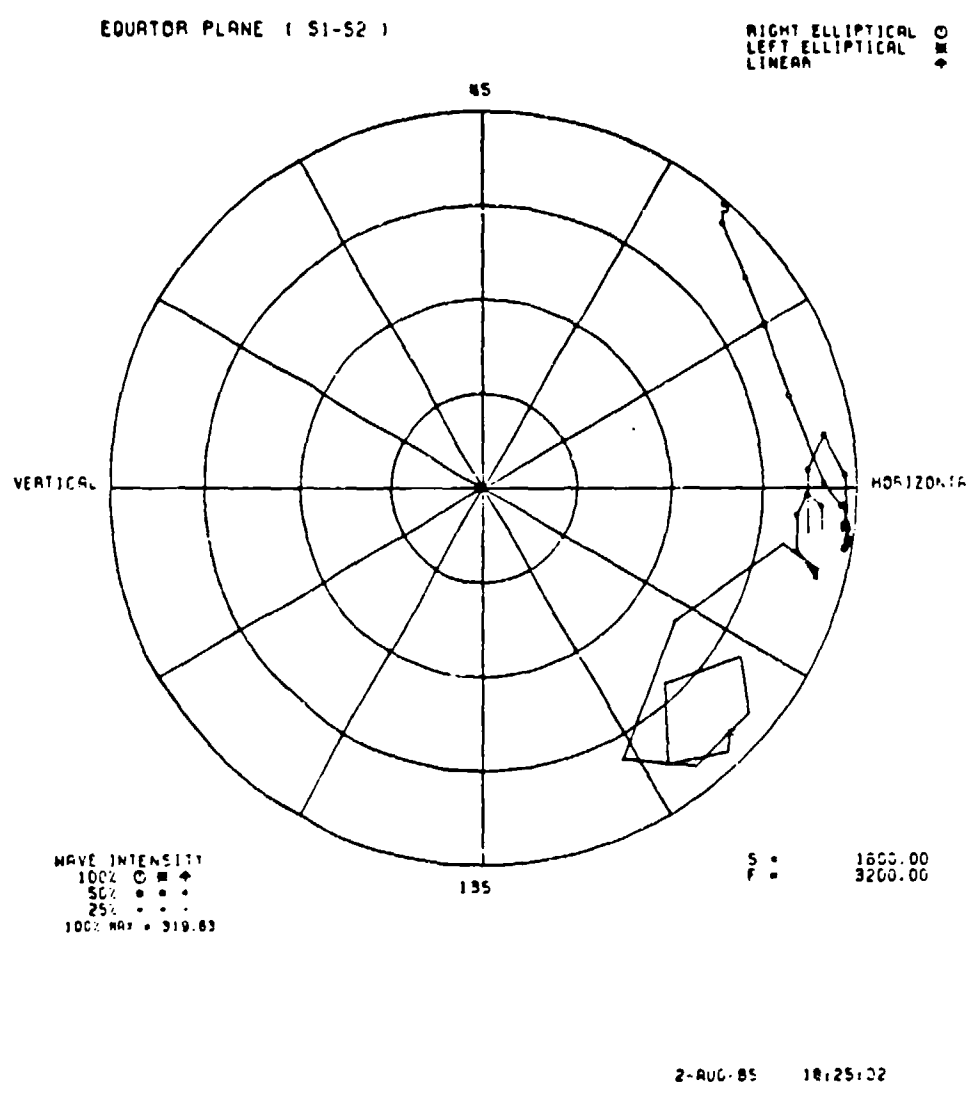

Figure 3.5. Polar projection of Poincaré sphere representation for Boeing 727 (band limited).

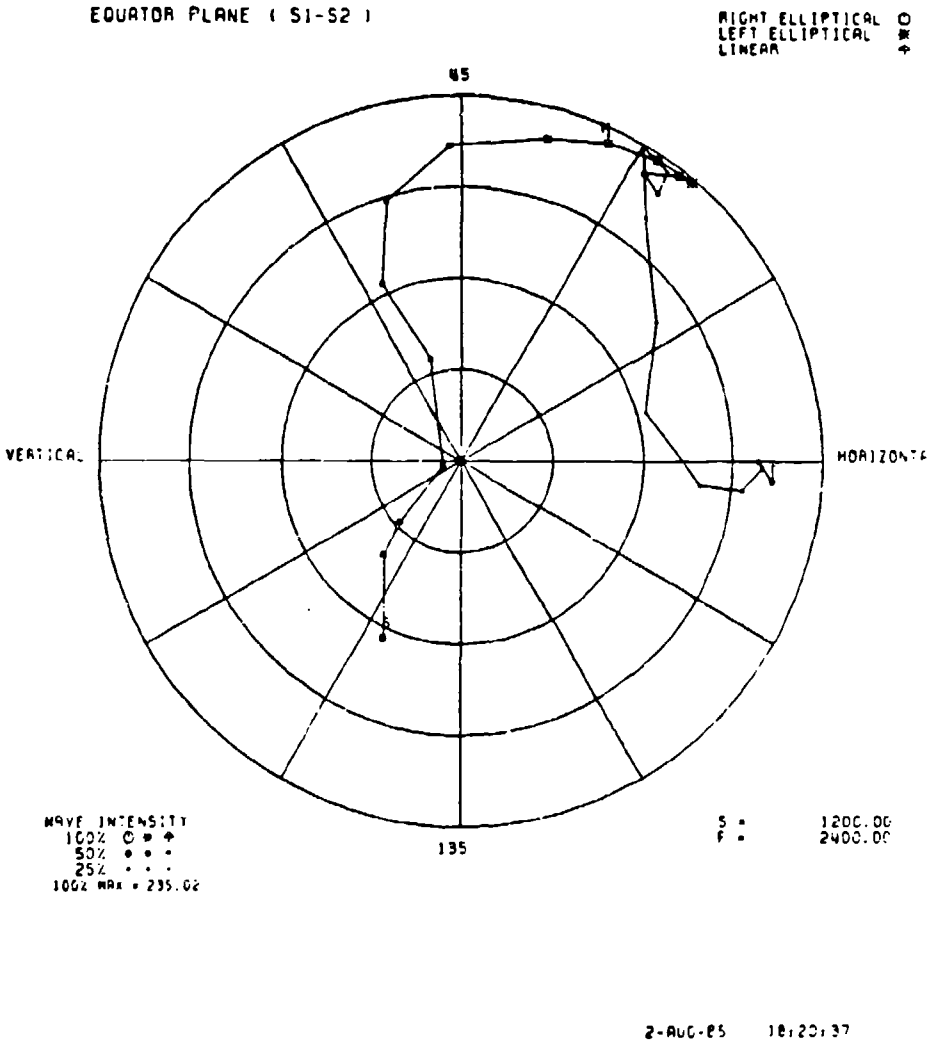

Figure 3.6. Polar projection of Poincaré sphere representation for Boeing 707 (band limited).

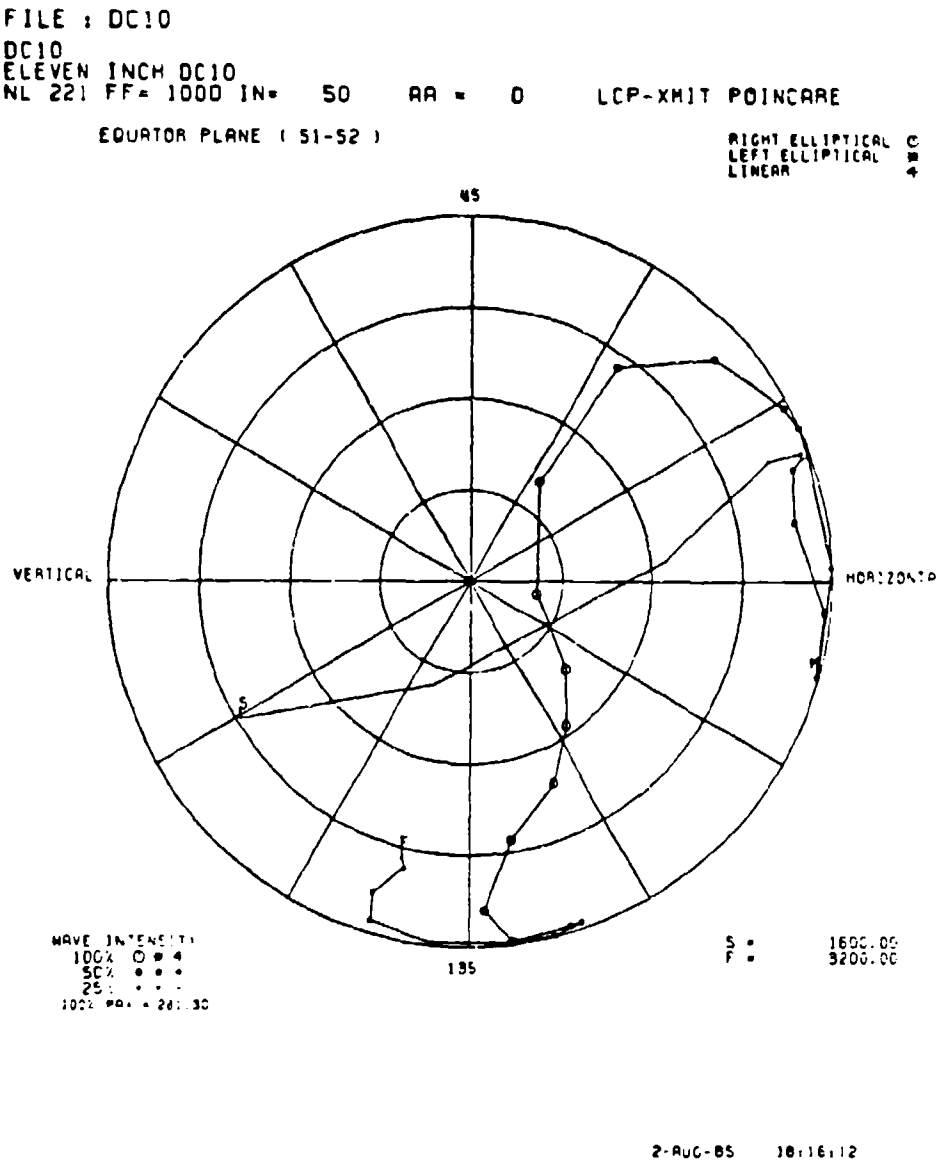

Figure 3.7. Polar projection of Poincaré sphere representation for DC10 (band limited).

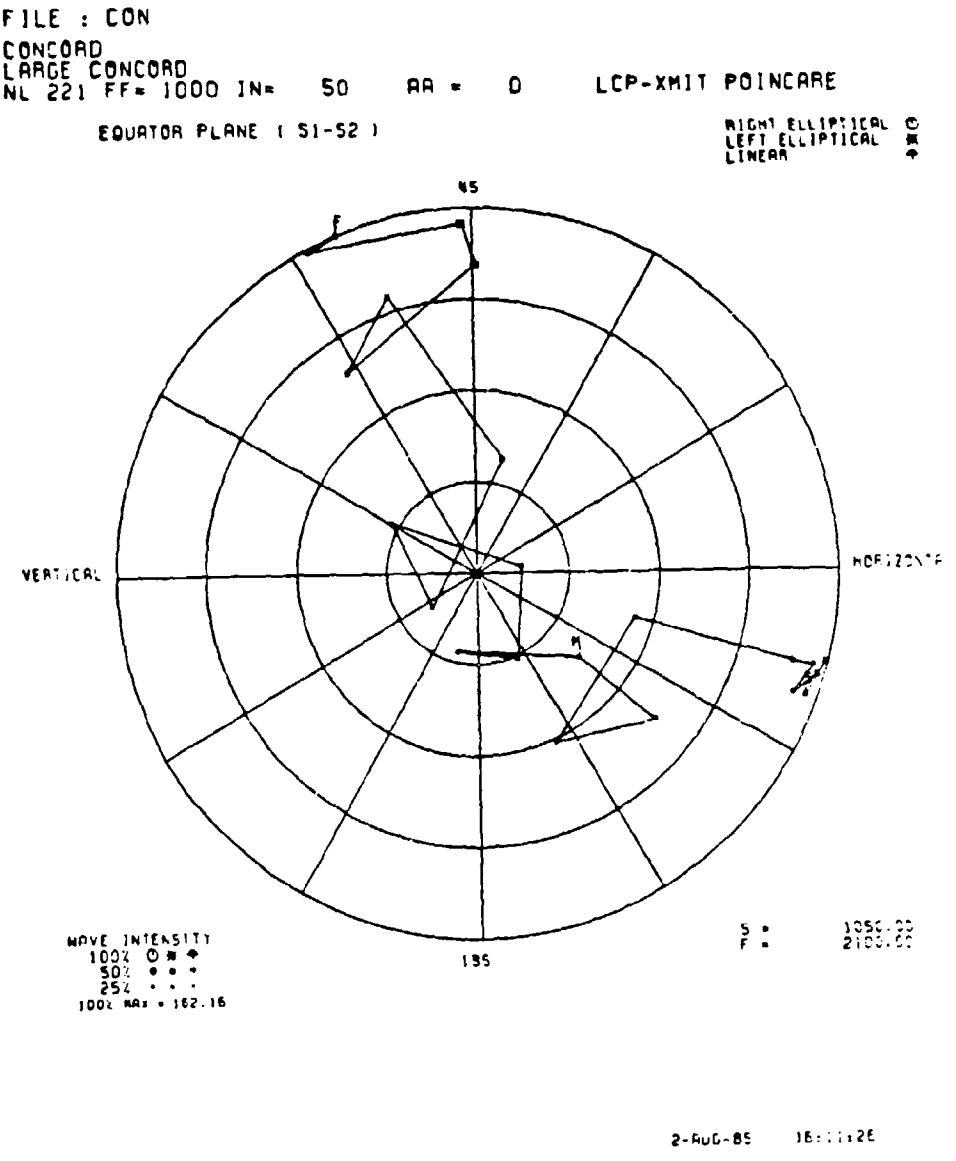

Figure 3.8. Polar projection of Poincaré sphere representation for Concorde (band limited).

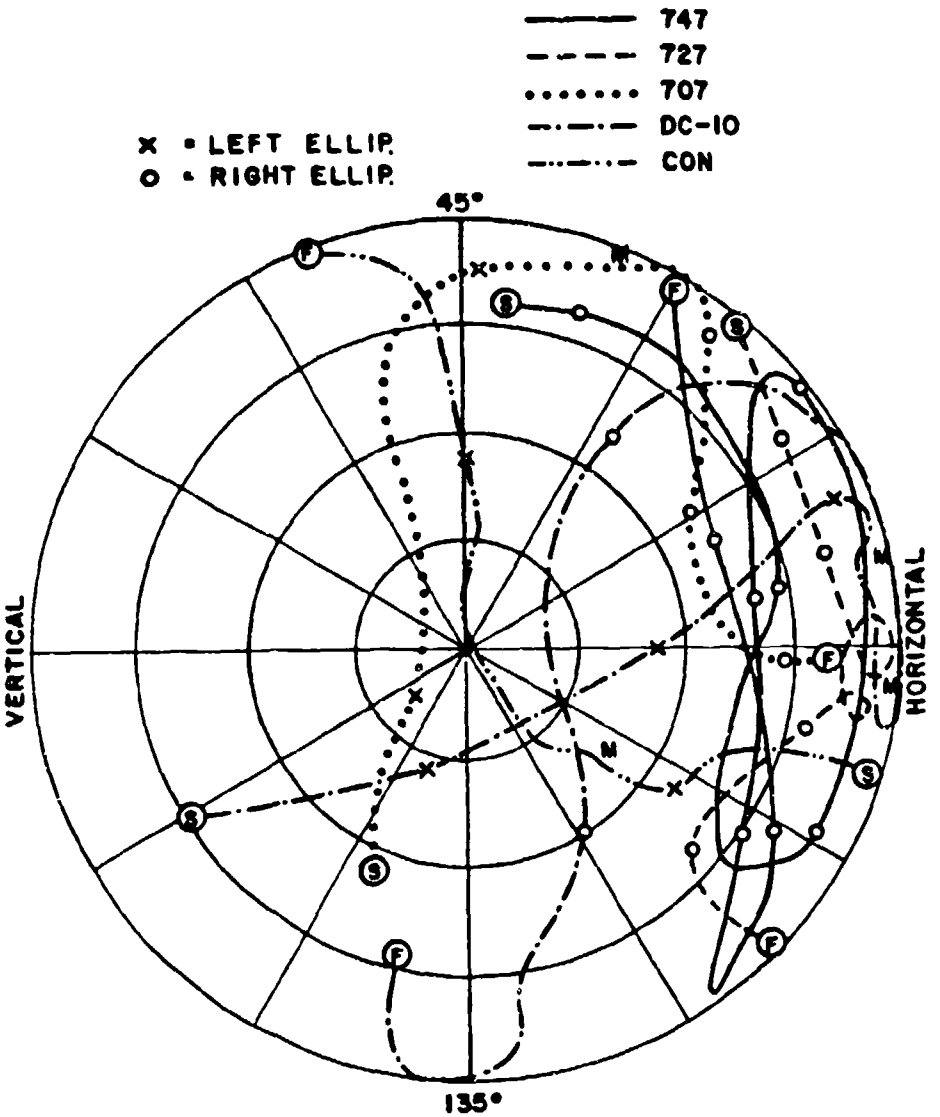

Figure 3.9. Polar projection of Poincaré sphere representation for all five aircraft (band limited).

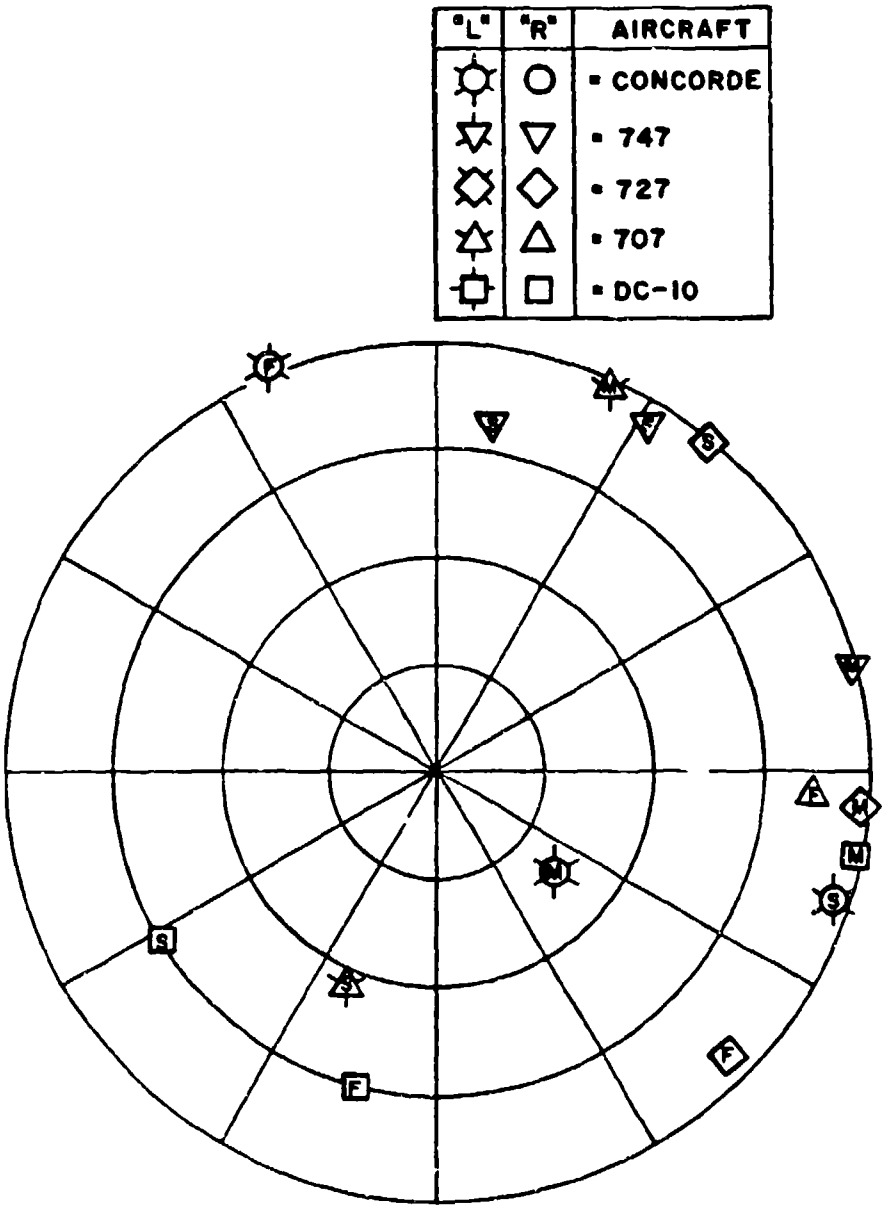

Figure 3.10. Polar projection of Poincaré sphere representation of RCS of five aircraft (selected frequencies).

automatic algorithms to perform this task and on a study of the sensitivity of such techniques to measurement errors in the raw data.

3.3 POLARIZATION FEATURES AND SIMULATION RESULTS

The initial investigation of the performance of target identification systems using polarization state data was based on the following sets of polarization parameters (all of which are easily derived from the linear-polarization scattering matrix coefficients $\underline{I}_{VV}$, $\underline{I}_{HH}$, and $\underline{I}_{VH}$):

Linear-polarization coefficients

1. VV Vertical-receive Vertical-transmit
2. HH Horizontal-receive Horizontal-transmit
3. VH Vertical-receive Horizontal-transmit

Circular-polarization coefficients

1. RR Right-hand-circular-receive Right-hand-circular-transmit
2. LL Left-hand-circular-receive Left-hand-circular-transmit
3. RL Right-hand-circular-receive Left-hand-circular-transmit

Axial-Ratio coefficients (see Section 3.2.1)

1. RAX Right-hand-circular-transmit axial-ratio
2. LAX Left-hand-circular-transmit axial-ratio

Polarization-Ratio coefficients

1. VV/HH Vertical-Vertical relative to Horizontal-Horizontal
2. VH/VV Vertical-Horizontal relative to Vertical-Vertical

Linear combinations of polarization coefficients; for constants a, b, and c

1. Linear aVV + bHH + cVH
2. Circular aRR + bLL + cRL

Concatenated combinations of polarization coefficients

1. Linear VV | HH | VH
2. Circular RR | LL | RL

Using these polarization parameter sets as "features" for the target identification algorithm, a series of simulation experiments were conducted for various ranges of parameters. A description of these experiments, along with a comparison of the most interesting results and a discussion of possible directions for future research are given below.

3.3.1 Experimental Approach

Let X_{ki} represent the complex normalized scattering coefficient of target k, for a particular combination of transmit and receive polarizations at transmit frequency f_i. (The term "complex normalized scattering coefficient" refers to a quantity whose magnitude is the square-root of the measured radar cross section in square meters and whose phase is the calibrated phase of the measured signal. The radar cross section of an object, and hence the square of the magnitude of the complex normalized scattering coefficient, is defined here in term of decibels relative to one square meter, i.e., in DBSM.) A set of N such measurements at discrete frequencies for target k at azimuth angle (ψ) and elevation angle (ν) may be represented by the complex vector.

$$X_k(\psi,\nu) = [X_{k1}(\psi,\nu),\ldots,X_{kN}(\psi,\nu)]^T \qquad (3.6)$$

A catalog of test targets (or prototypes) is obtained by entering a set of measurements for each of the five aircraft, for each polarization type, azimuth angle, and elevation angle of interest into a data base [2]. For this particular set of experiments, measurements in the 8-58

MHz scaled-frequency band were available for each of the aircraft at 10° increments of azimuth angle and for the three linear polarization types discussed above.

3.3.1.1 Noise Model

The noise model employed in this initial investigation was the additive white Gaussian noise model. In particular, a complex-valued vector of measurements representing the measurement of a radar return, Y from an "unknown" target was simulated by forming the complex vector sum

$$Y = X + N \tag{3.7}$$

of one of the set of cataloged target vectors and a vector of complex-valued Gaussian deviates $N = [N_1, N_2, \ldots, N_N]^T$. The "independent" complex-valued Gaussian deviates were generated by forming the complex vector sum, $N_i = A_i + jB_i$, where $j = \sqrt{-1}$, and where the zero-mean, σ^2-variance Gaussian deviates A_i and B_i were computed using the methods discussed in Abramowitz and Stegun [5]. The noise model is completed by the specification of the variance (or, average power), $2\sigma^2$ of the individual complex Gaussian deviates N_i. For the present investigation, the average noise power was specified in absolute terms, in units of DBSM. Some of the reasons for adopting this method of specifying the average power of the additive noise process are discussed below.

It is common practice in the radar literature to consider the performance of a target detection system as a function of a signal-to-noise ratio (SNR); thus normalizing the average power of the additive noise with respect to the total power of the desired signal. While this parameter is a reasonable "benchmark" parameter for target detection systems, a performance evaluation of target identification systems based upon a specification of noise power that is dependent on the a-priori unknown amplitude of the measured signal may be misleading in some cases. For example, it seems unreasonable to expect an increased level of noise to be present during the interrogation of a large-cross-section target, relative to the level for a target with small radar cross section.

Other reasons for this choice of "normalization" include the fact that signal-independent specification of noise power most accurately represents systems in cases where internal or "front-end" noise is the dominant source of measurement errors. Indeed, the noise power in DBSM may be computed directly in terms of the "noise temperature" or "noise figure" of the radar reciever.

In addition, an absolute reference for noise power allows a fair comparison of the performance of systems employing different polarization coefficients as features. For example, the Right-circular-recieve, Right-circular-transmit (RR) coefficient could be measured either directly, using right-circular transmit and receive antennas; or indirectly, using both horizontal and vertical transmit and receive antennas and forming the vector quantity

$$Y_{RR} = \frac{Y_{HH} - Y_{VV}}{\sqrt{2}} - jY_{VH} \qquad (3.8)$$

Assuming that comparable components are used to build each system, there should be no advantage, in terms of immunity to additive noise, inherent in either design.

The issue of fair comparisons is of even more concern when evaluating the performance of identification algorithms based on features involving polarization coefficients that are nonlinear combinations of measured quantities. In particular, consider the formation of an axial-ratio component vector from Right-circular, Right-circular (RR), and Right-circular Left-circular (RL) measurements, viz.

$$Y_{AR} = \left| \frac{|Y_{RR}| - |Y_{RL}|}{|Y_{RR}| + |Y_{RL}|} \right| . \qquad (3.9)$$

Clearly, it is not appropriate to specify the average power of an additive noise component in the original measurements based on the magnitude of an axial-ratio value; nor would it be appropriate to totally neglect the effects of "front-end" noise, even if the measured signal is moderately strong.

3.3.1.2 Distance Metrics

As discussed above, one of the objectives of this investigation was the determination of the value of precise phase information in the identification process. This was accomplished by comparing the results of experiments using a "coherent" (complex) distance metric,

$$d_c(Y,X) = \|Y-X\|^2 \tag{3.10}$$

to those using a "non-coherent" (magnitude) distance metric,

$$d_n(Y,X) = \|\,|Y| - |X|\,\|^2 \tag{3.11}$$

where $|Y|$ denotes a vector whose components are the magnitudes of the complex-valued components of the vector Y.

3.3.1.3 Identification Algorithm

The identification algorithm employed in this study was the single nearest-neighbor algorithm. The nearest-neighbor algorithm anounces target identity i (where i represents one of the targets in the catalog set) if

$$i = \arg\min d(Y,X_k) \; ; \; k = 1, 2, 3, \ldots, k \tag{3.12}$$

If the target identity i does not match the identity of the catalog target used to simulate the return of the unknown target, an error is charged to the experiment. By performing many such experiments, using independent noise deviates for each test, a cumulative sum of errors may be computed for each test target (posing as an "unknown" target), and for each level of average noise power of interest.

3.3.2 Results

The results of this study support the following hypotheses:

* For most of the polarization features considered, the use of precise phase information produces significant performance

gains (on the order of 10dB). Somewhat surprising, however, is the fact that an identification error rate as low as 0.1 (10%) can be achieved at a SNR of about 0dB when phase information is available.

* Of the polarization types tested, the linear co-pole features (HH and VV) and features primarily consisting of linear combinations of linear co-pole measurements (RCP, LCP, and RLCP) allowed the most reliable identification.

* The tests indicate that the overall performance is most error-free at azimuth angles near 90° (broadside). While this result is not surprising, it is not totally in agreement with the results of previous simulation studies that were based on SNR noise power normalizations.

* For this type of noise model, features that are nonlinear transformations of (noisy) measurements, such as axial-ratios, are <u>not</u>, in themselves, reliable features.

It should be emphasised that these data represent only a <u>preliminary</u> investigation, and the results cited herein should be considered as inconclusive.

CHAPTER 4

COMPLEX NATURAL RESONANCE EXTRACTION FROM CROSS-POLARIZED MEASURED SCATTERING DATA

4.1. INTRODUCTION

The complex natural resonances (CNR's) of an object are useful for identification purposes. The success of this procedure, however, depends on careful extraction of the CNR's as well as the identification process. In this chapter, the emphasis is on the resonance extraction process itself and we illustrate the usefulness of cross-polarized scattering data in this context. The availability of accurate, broadband scattering data has made the present study possible [1]. At most orientation angles the cross-polarized returns are at least ten dB below the co-polarized returns but the data are still useful for natural resonance extraction. In fact, a very dominant specular return in the co-polarized data usually masks the resonance effect. This is found to be the case for aspects near broadside for the aircraft. For both the co-polarized and cross-polarized data the method of CNR extraction is the rational function fit method [3]. The targets are electroplated models of modern aircraft.

4.2. THEORETICAL BACKGROUND

For simple objects such as the sphere and infinite circular cylinder, rigorous analytical solutions exist for the location (in the complex s plane) of the CNR's. For geometrically complicated targets, however, the CNR's must be extracted from measured scattering data. Even modest electrical sizes cannot be treated using a moment method formulation and numerical search procedure.

A scatterer has an infinite number of CNR's and is therefore a system of infinite order. The impulse response of a geometrically simple target or, for that matter, the response of the target to any aperiodic illumination, consists of first a forced response as the wavefront moves across the target and then a free or natural response as the wavefront moves beyond the target. As discussed later, the separation is not distinct for complicated targets. In the s (Laplace) domain then the transfer function of the target can be modelled as a residue series plus an entire function.

$$F(s) = \sum_{n=1}^{\infty} \frac{C_n(\Omega)}{s - s_n} + G(s,\Omega) \qquad . \qquad (4.1)$$

The C_n's are the residues which are aspect (Ω) dependent, the s_n's are the natural resonances and $G(s,\Omega)$ is the entire function. Note that the entire function is also dependent on aspect.

Any practical measurement system is a bandlimited system so only a limited number of CNR's are significant for calculations in a particular frequency range. The response to an impulse input is actually of the form

$$Y(s) = \sum_{n=1}^{N} \frac{C_n}{s - s_n} + \hat{G}(s,\Omega) + N(s) \quad , \qquad (4.2)$$

and

$$y(t) = \sum_{n=1}^{N} C_n e^{s_n t} + \hat{g}(t,\Omega) + n(t) \quad , \qquad (4.3)$$

where $\hat{G}(s,\Omega) = \begin{cases} G(s,\Omega) & \text{within passband} \\ 0 & \text{outside passband.} \end{cases}$

In a practical system one obtains the response as a function of real frequency, corresponding to information over a certain region of the jω axis. Neglecting the noise for the moment, if the unknowns of Equation (4.2), i.e. C_n, s_n and $G(s,\Omega)$ can be found somehow, the equation suggests that one has knowledge of the portion of the complex s plane delineated by the real frequency limits. For geometrically complicated targets there is no known method for finding the entire function $G(s,\Omega)$. Therefore, some sort of approximating function must be employed in searching for the CNR's. Since the known data points are all on the jω axis, one is really performing an extrapolation even though complete knowledge of the entire function is not the goal. For this reason no method of CNR extraction can claim absolute accuracy. The entire function part of the response, being unknown and aspect dependent, causes difficulties. In Prony's method, where the time-domain response is sampled, it has been suggested that the late-time portion of the response be sampled [6]. With this approach the forced response portion of the return is avoided. This is possible for simple target shapes although the return may be many dB down. For complicated targets,

however, the response in the time domain is really a very complicated combination of free response and forced response. Some substructures of the target are resonating long before the interrogating wavefront moves beyond the target. The authors agree with Felsen [7] that subtracting the physical optics approximation would be a good first step to negate the effects of the entire function. Unfortunately, for geometrically complicated targets obtaining the physical optics approximation could be a major effort. We offer an alternative approach as outlined below.

The rational function is written as

$$F(s) = \frac{b_o + b_1 s + b_2 s^2 + \ldots + b_{N+1} s^{N+1}}{1 + a_1 s + a_2 s^2 + \ldots + a_N s^N} \quad , \quad (4.5)$$

rewriting Equation (4.5)

$$F(s) = \sum_{n=1}^{N} \frac{\tilde{C}_n}{s - s_n} + a + bs \quad , \quad (4.6)$$

where $b = \frac{b_{N+1}}{a_N}$ etc.

The expression a + bs in Equation (4.6) is a simple attempt to model the entire function. It is motivated by the fact that the impulse response of a number of simple objects have impulse or doublet singularities. Therefore, as long as the frequency range over which one extracts CNR's is not too large (the optical range is avoided) the approximation remains good. The unknowns a and b are both aspect and frequency range dependent.

A distinction should be made between the complex natural resonances of the target and the zeros of the denominator of Equation (4.5). The poles of Equation (4.5) are not necessarily true CNR's as there are usually curve fitting poles which must be eliminated. For a geometrically complicated target the true CNR's will not always appear in each test because certain of the resonances may be unexcited or only weakly excited for particular orientations of the target.

Equation (4.6) does not account for the different time delays for various components of the specular returns. Furthermore, these time delays are also aspect dependent. A possible formulation is as follows:

$$F(s) = \sum_{n=1}^{N} \frac{\tilde{C}_n}{s-s_n} + \sum_{i=1}^{I} (a_i e^{-g_i s} + b_i s e^{-h_i s}) \quad . \qquad (4.7)$$

The parameters g_i and h_i are real numbers that are aspect dependent. Equation (4.7) introduces more unknowns and is actually nonlinear. It may, however, lead to an even better fit of the measured spectrum. The individual time delays only change the phase of the corresponding specular terms. However, the time delays of Equatic (4.7) would affect the magnitude of F(s) also. Therefore, the use of an algorithm that requires only magnitude information will not offer any improvement. One way to remove the non-linearity is to estimate a priori g_i and h_i. This would require data which is sufficiently broadband that impulse and doublets with delay could be discerned. It would also require aspect and geometrical information of the object. The series expansion of the exponential terms is not useful since it may not converge.

Details of the application of the rational function method are given in [3]. Note that all of the coefficients in Equations (4.5) and (4.6) are real. Therefore the set of poles consists primarily of complex conjugate pairs with corresponding complex conjugate residues.

The form of Equation (4.6) can lead to a different method of target identification as given in [8]. With the method of identification given in [8], a and b play an important role and the identification technique is aspect dependent. For a given set of CNR's and a given frequency range, one first finds the ranges of variation of a and b for different signal to noise ratios. These parameters as well as the CNR's are stored. Given frequency scattering data from an unknown target, the set of CNR's are used to obtain the a and b of Equation (4.6) and are then compared to their corresponding ranges of variation to make a decision on the identity of the unknown target. This method actually takes advantage of the existence of the entire function and works extremely well for high (>15 dB) signal to noise ratios. For signal to noise ratios lower than 15 dB, the variation of a and b become too great for the method to be useful in its present form.

We now have a basic understanding of the theory of CNR extraction and are ready to examine the results of CNR extraction using co-polarized and cross-polarized scattering data.

4.3. COMPUTATION AND ANALYSIS

The specular portion of the backscatter response from geometrically complicated targets is predominantly in the co-polarized component. For all but the most anomalous target one can safely conclude that only a weak entire function component exists in the cross-polarized return. As will be demonstrated, this means better numerical stability for the CNR's extracted from the cross-polarized returns.

The compact radar cross section measurement range [1] was used to obtain calibrated amplitude and phase scattering data for the targets. A digital filter is then used to numerically time gate and remove unwanted clutter from the time regions where the target return is known to be zero. The time response of the target is not altered. Figure 4.1 shows a plot of the cross-polarized frequency response of an aircraft target at broadside incidence (90°). Figure 4.2 is the corresponding band-limited impulse response of the aircraft. In Figures 4.1 and 4.2 vertical polarization was transmitted and horizontal polarization was received. Figures 4.3 and 4.4 show corresponding frequency and time domain plots after the data have been passed through a digital filter. The purpose of the filter is to somewhat smooth the data without removing any salient features. The data shown in Figure 4.3 are then used for pole extraction. Equation (4.5) is used to fit portions of the spectrum, typically applied over a 1.0 GHz bandwidth. This is done because of the extrapolation nature of the calculations. A wider bandwidth is not desirable from a theoretical viewpoint because windowing must be used to help eliminate pattern-fitting poles.

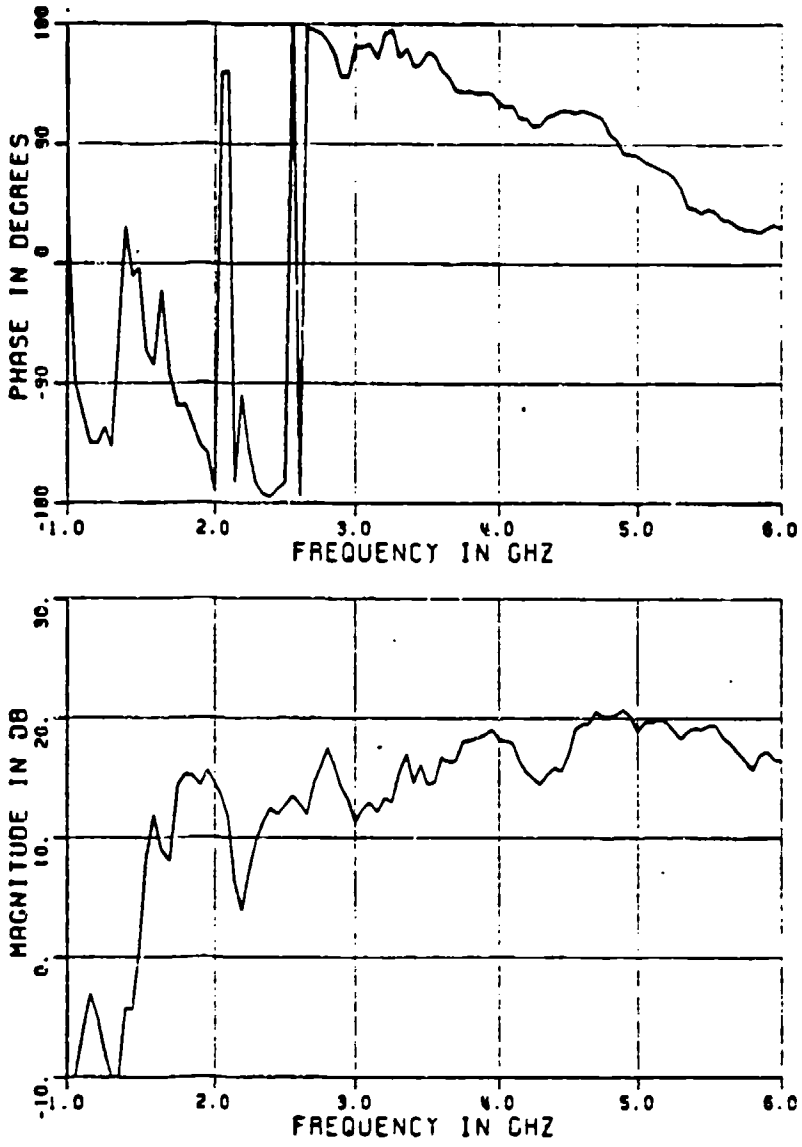

Figure 4.1. Cross-polarized amplitude and phase response of aircraft at broadside (90°).

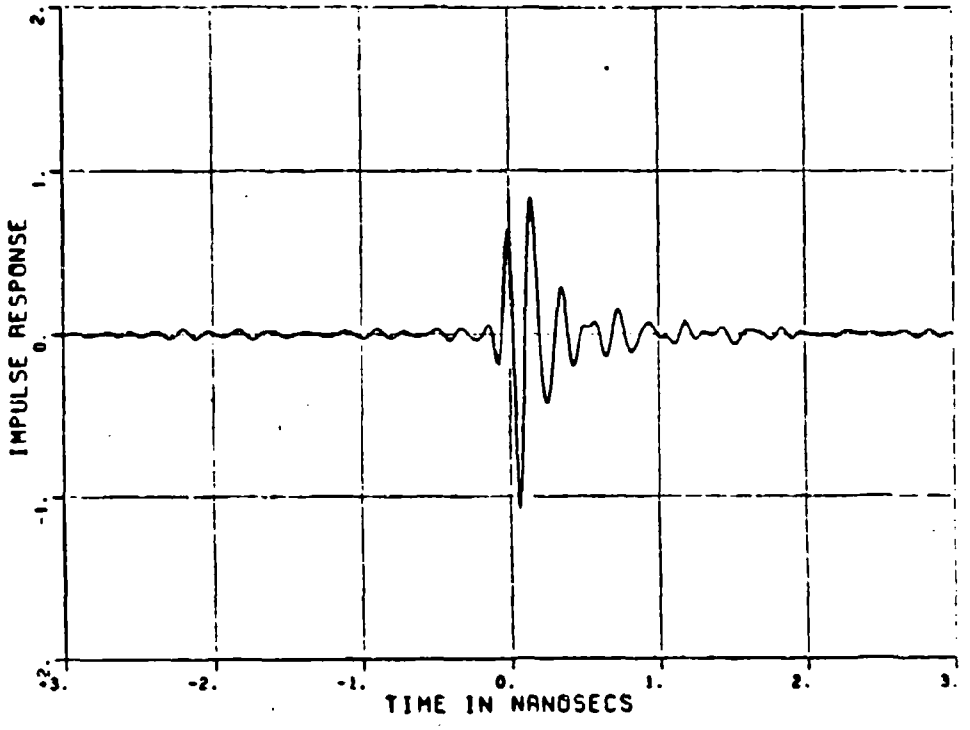

Figure 4.2. Cross-polarized impulse response of aircraft at broadside (90°).

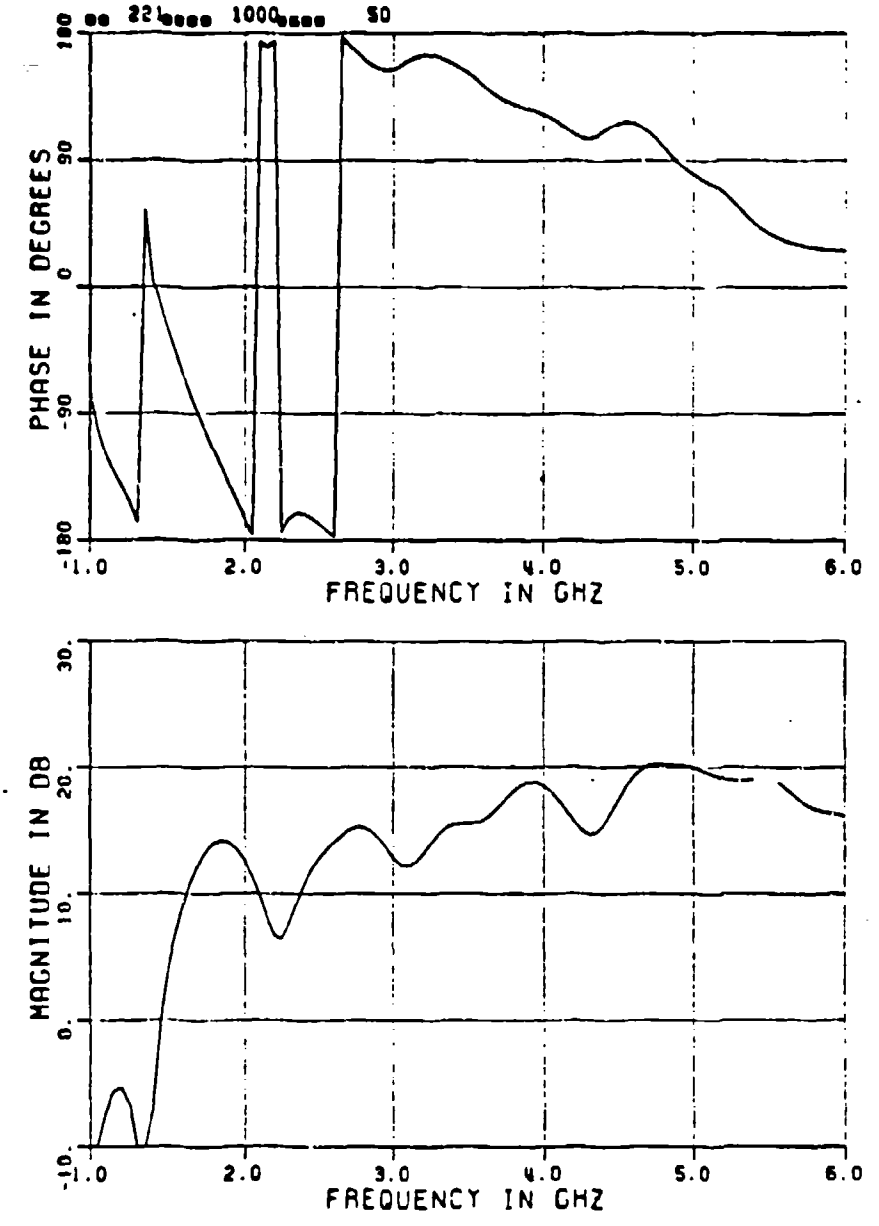

Figure 4.3. Cross-polarized amplitude and phase response of aircraft at broadside (90°) after digital filtering.

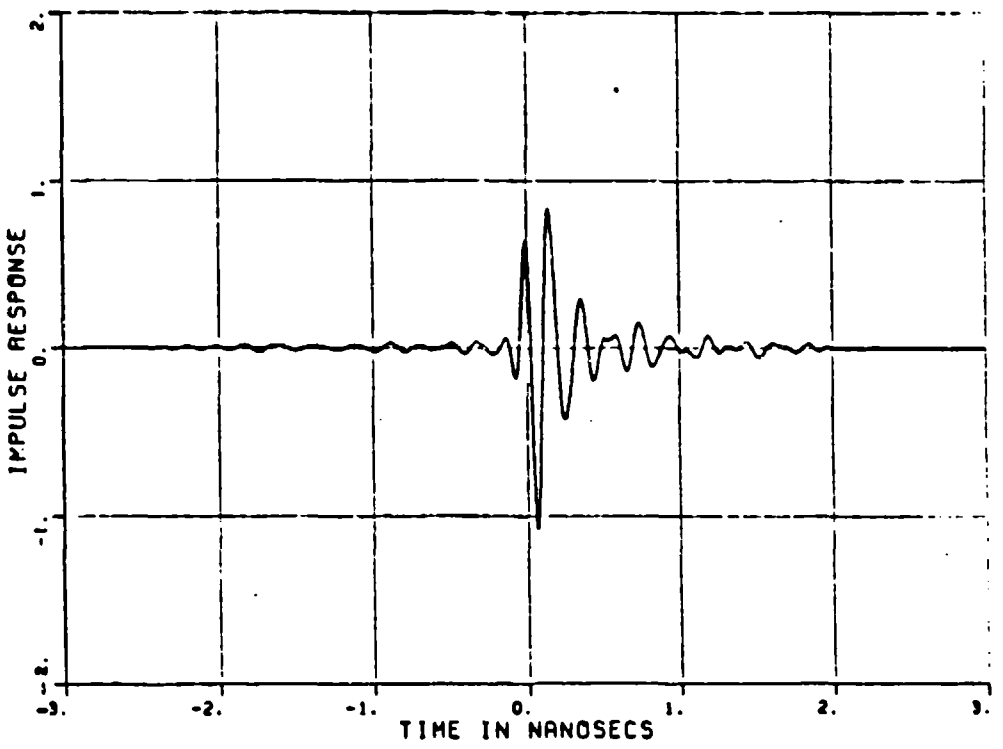

Figure 4.4. Cross-polarized impulse response of aircraft at broadside (90°) after digital filtering.

Choosing endpoints of the band at local minima helps to increase the accuracy of the solution. Slightly shifting this band, e.g., using 4.0 to 5.0 GHz and then using 4.05 to 5.05 GHz helps in weeding out curve or pattern-fitting poles.

CNR's have been extracted for four incidence angles 0° (nose-on), 45°, 90° and 180°, using three polarizations (vertical-vertical, horizontal-horizontal and vertical-horizontal). The CNR's extracted are listed in Table 4.1. Only the oscillatory part of the CNR's are listed.

It is clear from Table 4.1 that no incidence angle yields all of the extracted poles, but the cross-polarized results have a lower rate of absenteeism than the co-polarized results. Reasoning with regard to the specular returns, it seems clear that even near nose-on and tail-on where the cross-polarized return is 10 dB down from the co-polarized returns it is still advantageous not to have to deal with specular components. In the neighborhood near broadside (90°), considerable difficulty was experienced in extracting CNR's from the co-polarized returns. This was anticipated as it is clear that the entire function is quite large in this region. Figure 4.5, which shows the vertical-vertical broadside return and Figure 4.6 which shows the horizontal-horizontal broadside return are both relatively flat compared to the cross-polarized return in Figure 4.3.

Table 4.2 lists the average CNR's as found over the four angles. Maximum deviation from the average over the angles are listed inside parentheses. Both of the co-polarized results are essentially equally different from the cross-polarized returns. Table 4.1 also shows that

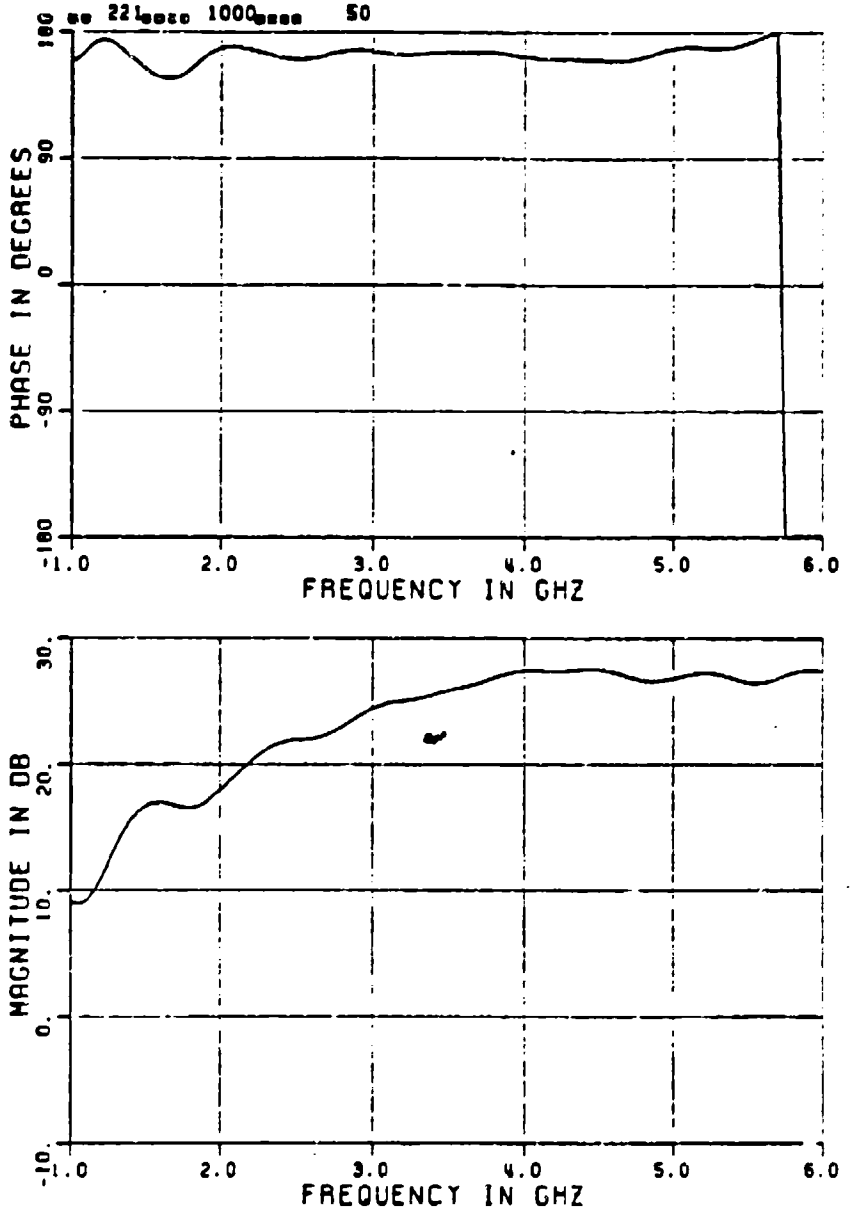

Figure 4.5. Vertically co-polarized amplitude and phase response of aircraft at broadside (90°) after digital filtering.

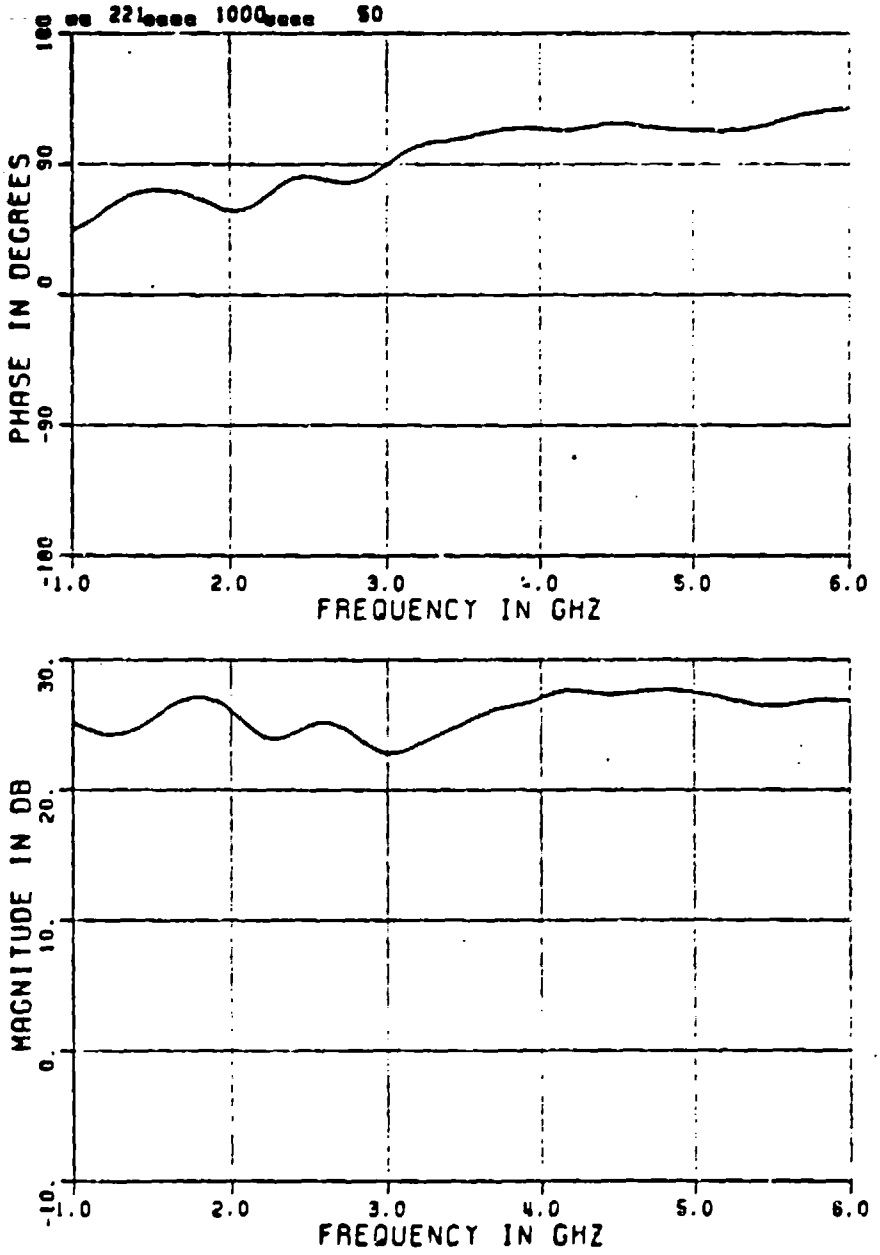

Figure 4.6. Horizontally co-polarized amplitude and phase response of aircraft at broadside (90°) after digital filtering.

TABLE 4.1

OSCILLATORY PARTS OF CNR'S EXTRACTED FROM BACKSCATTER

RESPONSES OF DIFFERENT POLARIZATIONS AND ANGLES

0°			45°			90°			180°		
VV	VH	HH	VV	VH	HH	VV	VH	HH	VV	VH	HH
---	1.143	1.017	1.215	1.134	1.106	1.259	1.050	1.090	1.208	1.198	1.100
1.408	1.470	1.474	1.494	1.574	1.626	1.427	1.490	---	1.473	1.488	1.439
1.642	1.682	1.770	1.765	1.797	---	1.714	1.821	1.742	---	---	---
---	1.956	1.958	1.919	---	2.097	---	2.015	2.128	2.097	2.038	1.926
2.330	2.195	2.280	2.210	2.247	2.418	2.420	---	---	2.298	2.341	2.233
2.720	2.512	2.592	2.657	2.656	2.717	---	2.647	2.643	2.657	---	2.597
---	2.905	3.073	2.965	2.871	---	2.947	3.065	---	3.047	2.970	---
3.310	3.287	---	3.298	3.271	3.276	3.349	---	---	---	3.321	3.219
3.586	3.747	3.654	---	3.707	3.675	---	3.639	3.781	3.645	3.572	---
4.026	4.059	4.159	3.893	4.067	---	3.971	4.103	4.113	4.100	4.021	4.145
4.192	4.239	---	---	---	4.208	---	---	---	4.226	4.241	---
---	4.718	4.543	4.627	4.727	4.684	4.717	4.671	---	4.596	---	4.510
---	---	5.056	---	5.024	5.136	---	---	---	---	4.924	4.796
5.442	5.505	5.533	---	---	---	5.51	5.547	5.511	---	5.677	5.622

TABLE 4.2

AVERAGE OF OSCILLATORY PARTS IN TABLE 4.1 OVER THE FOUR ANGLES

MAXIMUM DEVIATION FROM THE AVERAGE VALUE IS SHOWN IN PARENTHESIS

VV	VH	HH
1.227 (.032)	1.131 (.081)	1.098 (.008)
1.451 (.043)	1.506 (.068)	1.513 (.113)
1.707 (.065)	1.767 (.085)	1.756 (.014)
2.008 (.089)	2.003 (.047)	2.027 (.101)
2.315 (.105)	2.261 (.080)	2.310 (.108)
2.678 (.042)	2.605 (.093)	2.637 (.080)
2.958 (.061)	2.928 (.137)	3.073
3.319 (.030)	3.293 (.028)	3.248 (.029)
3.616 (.030)	3.666 (.094)	3.703 (.078)
3.998 (.105)	4.063 (.042)	4.139 (.026)
4.209 (.017)	4.240 (.001)	4.208
4.647 (.070)	4.705 (.034)	4.579 (.105)
---	4.974 (.050)	4.996 (.200)
5.476 (.034)	5.576 (.101)	5.555 (.067)

the co-polarized returns are more aspect dependent in that more poles are missing at many aspects compared to the cross-polarized returns. As would be expected for a complicated object, all of the poles shown in the cross-polarized returns are also present in one of the two co-polarized results. The cross-polarized returns cannot contain any CNR's that are not in any of the co-polarized returns.

4.4. USE OF HIGHER FREQUENCY DATA

The rational function method has been applied to the horizontal polarization response of another aircraft model at 6.0 - 12.0 GHz. The CNR's (TABLE 4.3) appear to have the same type of behavior as those found earlier using 1.0 - 6.0 GHz data. Therefore, this suggests that this frequency range is also one where it is meaningful to extract CNR and to use them for discrimination.

It is difficult to relate these resonances to structural features of the aircraft at this stage. It is possible to postulate physical substructures that resonate. However, there is no analytical proof. Also, each physical substructure would have more than one complex natural resonance associated with it. One possible way to discern structural dependence would be to use absorbing material on the various substructures to study their effect on the CNR's.

4.5. CONCLUSIONS FROM THE COMPLEX NATURAL RESONANCE STUDY

The practical implications and problems of CNR extraction have been studied using both co-polarized and cross-polarized backscattering data. The CNR extraction method and the required accuracy are directly related to target identification using prediction-correlation. The CNR locations must be quite accurate. The research reported here has demonstrated two main points. First, the frequency range which was used in previous studies can be doubled without encountering problems with the CNR concept. It is known that above some unknown high frequency limit the density of the CNR's will preclude target identification using prediction-correlation. Additional research is needed to establish this high frequency limit for practical targets. Second, it has been demonstrated that there are advantages in terms of orientation sensitivity and stability to CNR extraction using cross-polarized backscatter data. The disadvantage is that the data may be as much as 10 to 15 dB down from the co-polarized return. This point must be carefully understood. One could simply use cross-polarized data for CNR extraction. In this case the measured scattering data are controlled and the measurements are clutter-limited, not noise-limited. The extracted CNR's could then be used in prediction-correlation processing using co-polarized and/or cross-polarized scattering data. The idea of target identification from CNR's using cross-polarized real world scattering data needs to be very carefully explored.

TABLE 4.3

OSCILLATORY PARTS OF CNR'S EXTRACTED FROM

HORIZONTAL POLARIZATION RESPONSE OF ANOTHER AIRCRAFT

AT 6.0 - 12.0 GHZ BETWEEN 0° AND 90°

0°	15°	30°	45°	60°	75°	90°
6.465	4.247	6.245	6.520	6.479	6.559	6.410
7.406	7.302	7.385	7.282	---	7.413	7.342
7.908	8.005	7.906	8.000	8.077	---	8.040
8.686	---	8.516	8.556	8.696	---	8.730
8.974	9.017	9.141	9.156	9.924	9.153	8.918
9.521	9.585	9.776	9.550	9.562	9.582	9.621
---	10.053	10.117	10.053	---	10.059	9.951
10.53	10.45	10.469	---	10.516	10.475	10.59
10.873	---	11.078	11.094	10.95	---	11.072

CHAPTER 5

CONCLUSIONS

A number of important conclusions can be given at this time.

First, the goal of development of a target identification data base and associated data base management system was achieved. This data base was specifically configured for the study of the resonance-region broad-band polarization matrix behavior of the series of commercial aircraft and naval ships on which data were available at the ElectroScience Laboratory. It is now possible to access the full polarization scattering matrix (amplitude and phase; co-polarized and cross-polarized; fully calibrated) of these ships and aircraft using a single computer file access system which permits the study of the behavior of these various targets for a number of polarization states and feature sets.

The polarization matrix data base was next used for the purpose of testing a number of target identificaiton concepts. Chapter three has shown the details of the results for tests where the backscattered return for a number of polarization states and ratios of polarization states were used as features in the target identification algorithms. In general, it was shown that co-polarized data from fully coherent radar systems (ie: systems where the relative phase of the returned signals could be measured as well as the amplitude) with multi frequency capability could perform very effectively. Signal-to-noise ratios of 0

to +10 DB in the final estimates of the RCS and relative signal phase for the various targets was shown to be sufficient for misclassification percentages less than 5 percent. (See chapter three.) Of particular note was that the introduction of the ability of the radar system to measure relative received signal phase would produce performance improvements (over an "amplitude-only" system) of as much as 10 DB.

The use of complex natural resonances (CNR) in a radar target identification system was also studied using this new data base system. CNR values were extracted from both co-polarized and cross-polarized measured scattering data. It was shown that natural resonances can be meaningfully utilized using the 6.0 to 12.0 GHZ data. This indicates that the 30 to 60 MHZ band (full scale) can be used for CNR radar target identification. It was also shown that if the co-polarized returns are dominated by specular scattering then there are significant benefits to the use of the cross-polarized data. In particular, increased stability of the measured resonances with respect to target orientation was demonstrated.

There are a number of important areas for future research which can be discussed at this point. First, the extension of these results into higher frequency bands should be studied. Data at higher frequencies (a factor of two) for some of the aircraft exist at this time and such data should be studied. In particular, the application of these concepts at higher frequencies may permit the use of such techniques on subcomponents of targets rather than the overall target. This area of research could become a major new area in itself.

New concepts in the utilization of extracted target resonances should also be explored. In particular, the application of alternate polarization states as input to the resonance extraction techniques may be appropriate.

New algorithms for the identification process also need to be studied. Optimization techniques have not been applied as of yet to the radar target features and the associated identification algorithms. The optimum frequency bands and polarization states for identification of specific target types has not been derived.

REFERENCES

[1] Walton, E. K. and J. D. Young, "The Ohio State University Compact Radar Cross-Section Measurement Range," IEEE Tran. on Ant. and Prop., vol. AP-32, No. 11, November, 1984.

[2] Kamis, A. D., E.K. Walton and F. D. Garber, "NCTR Software Development Documentation," Technical Report 716559-1, The Ohio State University ElectroScience Laboratory, Columbus, Ohio, July, 1985.

[3] D.L. Moffatt and C.Y. Lai, "Natural Resonance Estimation," IEEE Trans. Instrumentation and Measurements, Vol. IM-34, No. 4, December 1985, pp. 547-550.

[4] W.M. Boerner et al. (eds.), Inverse Methods in Electromagnetic Imaging, 1985 D. Reidel Publishing Company, Dordrecht, Boston and Lancaster.

[5] M. Abramowitz and I.A. Stegun, ed. Handbook of Mathematical Functions, National Bureau of Standards, Washington, DC, 1965 (see especially Sec. 26 "Numerical Methods" pp. 949-953).

[6] J.R. Auton, T.L. Larry, and M.L. Van Blaricum, "Target identification via complex natural resonance extraction from radar signatures", NATO/AGARD "Target Signature" Symposium, October 8th-12th, 1984, London, England.

[7] L.B. Felsen, "Comments on Early Time SEM," IEEE Trans. Antennas Propagation, Vol. AP-33(1), January 1985, pp. 118-120.

[8] D.L. Moffatt and C.Y. Lai, "Non-cooperative Target Recognition," Ohio State University ElectroScience Laboratory Report 714190-12, to be published 1986.